



## A broadband perfect metamaterial absorber with angle-insensitive characteristics

Cang Liang, Xianglin Kong, Fengjun Wang, Ruofeng Xu, Yixiang Fu, Xiaoyu Pang, Shengjun Zhang, Xiaopeng Shen & Lei Zhao

To cite this article: Cang Liang, Xianglin Kong, Fengjun Wang, Ruofeng Xu, Yixiang Fu, Xiaoyu Pang, Shengjun Zhang, Xiaopeng Shen & Lei Zhao (2022): A broadband perfect metamaterial absorber with angle-insensitive characteristics, Journal of Electromagnetic Waves and Applications, DOI: [10.1080/09205071.2022.2143297](https://doi.org/10.1080/09205071.2022.2143297)

To link to this article: <https://doi.org/10.1080/09205071.2022.2143297>



Published online: 09 Nov 2022.



Submit your article to this journal [↗](#)



View related articles [↗](#)



View Crossmark data [↗](#)

RESEARCH ARTICLE



## A broadband perfect metamaterial absorber with angle-insensitive characteristics

Cang Liang<sup>a</sup>, Xianglin Kong<sup>a</sup>, Fengjun Wang<sup>b</sup>, Ruofeng Xu<sup>a</sup>, Yixiang Fu<sup>c</sup>, Xiaoyu Pang<sup>c</sup>, Shengjun Zhang<sup>b</sup>, Xiaopeng Shen<sup>d</sup> and Lei Zhao<sup>a</sup>

<sup>a</sup>School of Information and Control Engineering, China University of Mining and Technology, Xuzhou, People's Republic of China; <sup>b</sup>Test Physics & Numerical Mathematical, National Key Laboratory of Science and Technology, Beijing, People's Republic of China; <sup>c</sup>High Performance Electromagnetic Window, Key Laboratory of Aeronautical Science and Technology, Jinan, People's Republic of China; <sup>d</sup>School of Materials Science and Physics, China University of Mining and Technology, Xuzhou, People's Republic of China

### ABSTRACT

A broadband perfect metamaterial absorber (MA) based on bilayer resistive films with different structure units is proposed in the microwave regime. An equivalent circuit model based on transmission line theory is established to guide the absorber design and explain its broadband and perfect absorption mechanism. The absorber characters high absorptivity and stable angular. The MA displays more than 98% absorption from 4.9 to 22.6 GHz at normal incidence. The performance is suitable for transverse electric (TE) and transverse magnetic (TM) waves at normal incidence, while absorption is better than 90% (80%) within the oblique incidence 50° (60°). The measured results of absorption and 10 dB radar cross section (RCS) agree well with the simulated ones.

### ARTICLE HISTORY

Received 1 September 2022  
Accepted 30 October 2022



### KEYWORDS

Metamaterial absorber;  
broadband; angular stability;  
high absorptivity

## Introduction

Microwave absorbers (MA) are widely used in electromagnetic shielding, wireless communication, imaging, and radar cross section (RCS) reduction to absorb and dissipate electromagnetic (EM) energy [1–5]. Salisbury screen and pyramidal absorbers have been successively proposed for wide bandwidth absorption, while the large weight [6] and low angular stability [7] limit their potential applications in many fields.

Metamaterial has become an attractive research direction owing to its special properties in electromagnetic fields. Metamaterial absorbers can remove energy from the electromagnetic waves by perfectly matching air impedance to achieve good absorption performance by consuming the energy of the incident EM waves [8–12]. In recent years, metamaterial absorbers have made great progress in polishing up the performance of broadband or oblique incidence. Resistive films were employed to accomplish a broadband absorber, obtaining more than 90% absorptivity from 6.06 to 14.66 GHz [13]. Multi-layer structure

**CONTACT** Lei Zhao  leizhao@cumt.edu.cn  School of Information and Control Engineering, China University of Mining and Technology, No.1 Daxue Road, Xuzhou, People's Republic of China

is employed to expand operating bandwidth, which achieves a bandwidth with absorption of 90% from 4.73 to 39.04 GHz [14]. To enhance the angular stability in oblique incidence, inkjet-printed conformal metamaterial absorber (MA) is proposed, which can achieve more than 90% absorptivity from 8.43 to 10.38 GHz for wide angular stability up to 45° [15]. A microwave MA using dispersion-engineer is characterized by more than 90% absorption within 2.11–3.89 GHz with the wide angular stability up to 50° [16]. A perfect absorber with more than 95% absorptivity is exceedingly important device in microwave region. Multipole absorber based on coupling interlayers is presented to gain more than 95% absorption from 5.5 to 6.5 GHz [17]. A conformal MA is designed to realize 95% absorptivity within 4.2–10.2 GHz [18]. The above studies only focus on the performance of broadband or widely oblique incidence or high absorption. It is a great challenge to design a perfect absorber with wide-angle stability and broadband operating bandwidth.

In this paper, we present a broadband angle-insensitive perfect absorber by using bilayer resistive films with different surface resistance, two dielectric substrates, and a ground layer. Bilayer resistive films and dielectric substrates are applied to provide resonance absorption peak and match air impedance to realize wideband absorption. The proposed absorber is fabricated by screen printing technology and measured. The proposed MA has the following advantages: (1) the design can provide over 98% wide absorption from 4.9 to 22.6 GHz (fractional bandwidth (FBW) of 128.7%) under normal incidence; (2) the MA is insensitive to oblique incidences within 60°; (3) it is applicable for TE and TM polarization.

## Design theory and methods

### Single and bi-layer absorber with RLC series and resistive film

A typical single-layer absorber has a loss layer at a certain distance above the conductive plate, which equivalent circuit model (ECM) is described in Figure 1(a). Figure 1(b) shows the first layer of the proposed absorber. A resistive film can be seen as an RLC ( $R_1$ ,  $L_1$ ,  $C_1$ ) series circuit [19], and  $Y_{RLC1}$  is the admittance of the equivalent circuit of square resistance film. The dielectric with the thickness of  $t_p$  and  $t_1$  can be considered a transmission line with equal length, respectively. And the ground plane can be treated as conducting wire. Its reflection coefficient can be calculated by

$$\Gamma = \frac{Y_0 - Y_{in}}{Y_0 + Y_{in}} \quad (1)$$

where

$$Y_{in} = Y_{RLC1} + Y_d \quad (2)$$

$$Y_{RLC1} = \frac{1}{R_1 + j\left(\omega L_1 - \frac{1}{\omega C_1}\right)} = G_1 + jB_1 \quad (3)$$

$$G_1 = \frac{\omega^2 R_1 C_1^2}{(1 - \omega^2 L_1 C_1)^2 + \omega^2 R_1^2 C_1^2} \quad (4)$$

$$B_1 = \frac{\omega C_1 - \omega^3 L_1 C_1^2}{(1 - \omega^2 L_1 C_1)^2 + \omega^2 R_1^2 C_1^2} \quad (5)$$

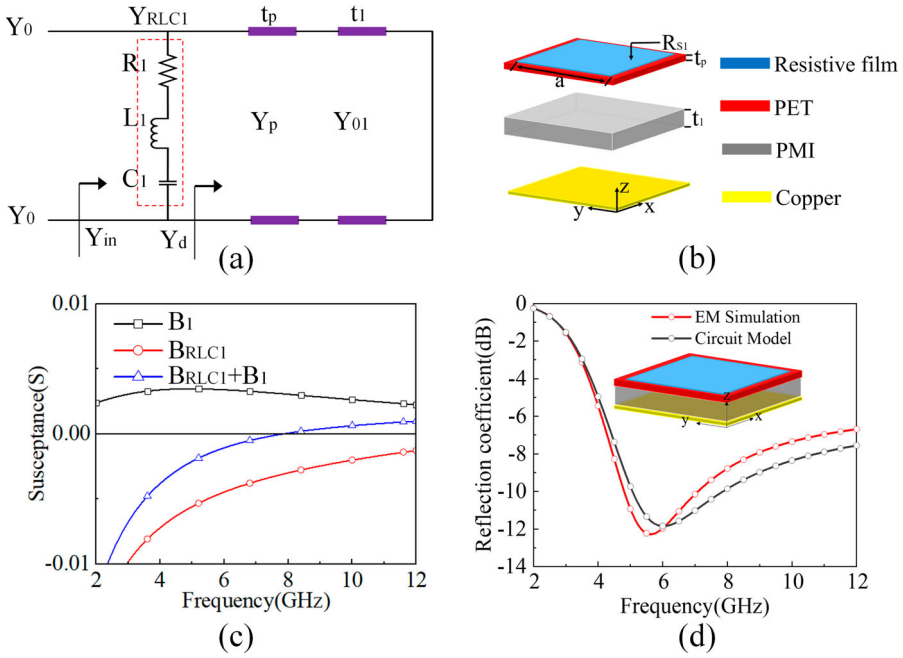


**Figure 1.** (a) Equivalent circuit model of single-layer absorber. (b) Configuration of the designed absorber. (c) Susceptance for the RLC series and dielectric. (d) The reflection coefficient obtained from EM simulation and ECM calculation are compared.

$$Y_d = j \frac{Y_p(Y_p \tan(\beta_p t_p) - Y_{01} \cot(\beta_1 t_1))}{Y_p + Y_{01} \cot(\beta_1 t_1) \tan(\beta_p t_p)} = jB_d \quad (6)$$

and  $Y_{01} = Y_0 \sqrt{\epsilon_1}$ ,  $\beta_1 = 2\pi \sqrt{\epsilon_1} / \lambda$ ,  $\beta_p = 2\pi \sqrt{\epsilon_p} / \lambda$ ,  $\omega = 2\pi f$ ,  $Y_0$  is the characteristic admittance of free space, and  $\epsilon_1$ ,  $\epsilon_p$  are relative permittivity.  $B_1$  is the susceptance of RLC series circuit.  $G_1$  is the conductance of RLC series circuit.

The typical input susceptance is shown in Figure 1(c). It is well known that resonance occurs at the time the input susceptance is zero [20]. In Figure 1(c), there is an obvious resonance frequency at  $f_{r1}$ . Then the absorption resonance can be obtained before the frequency at  $f_{r1}$ . The reflection curves of the designed single-layer absorber obtained by using ECM and full-wave simulation are illustrated in Figure 1(d), which have a good agreement. The circuit dimensions are  $R_1 = 144 \Omega$ ,  $L_1 = 0.1 \text{ nH}$ ,  $C_1 = 0.219 \text{ pF}$ , respectively.

To expand the absorption bandwidth, an ordinary method is introduced by overlaying an extra lossy layer on the original layer to provide another absorption resonance. The specific circuit and structure of the proposed absorber are shown in Figure 2(a,b). For two-layer ECM shown in Figure 2(a), input admittance can be calculated as following formulas.

$$Y_{RLC,i} = \frac{1}{R_i + j \left( \omega L_i - \frac{1}{\omega C_i} \right)} = G_{RLC,i} + jB_{RLC,i}, i = 1, 2 \quad (7)$$

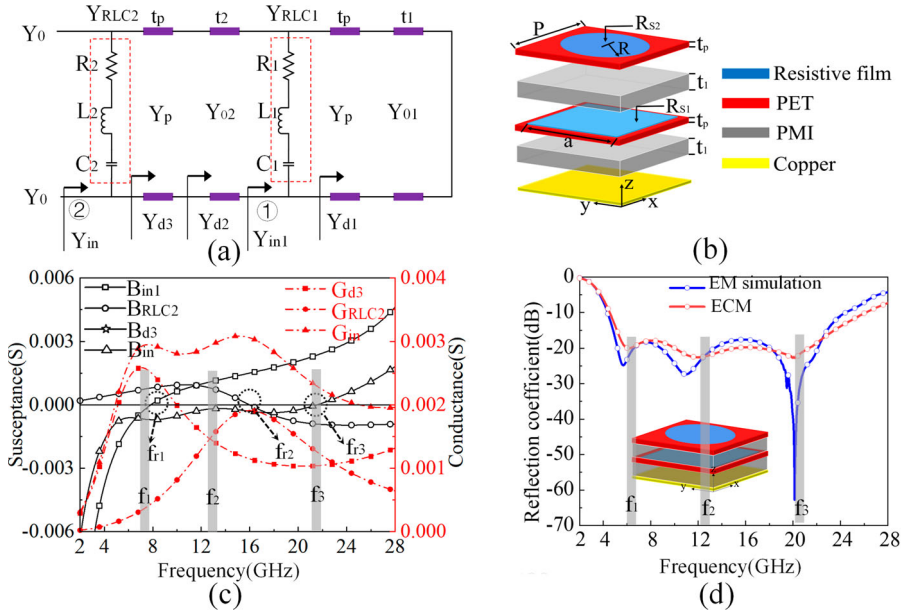


**Figure 2.** (a) Equivalent circuit model of bi-layer absorber. (b) Schematic diagram of the designed absorber. (c) Calculated imaginary parts with  $B_{in1}$ ,  $B_{RLRC2}$ ,  $B_{in}$  and real parts with  $G_{d2}$ ,  $G_{RLRC2}$ ,  $G_{in}$ . (d) Comparison of the reflection coefficient obtained by EM simulation and ECM calculation of two layers.

$$Y_{d1} = j \frac{Y_p(Y_p \tan(\beta_p t_p) - Y_{01} \cot(\beta_1 t_1))}{Y_p + Y_{01} \cot(\beta_1 t_1) \tan(\beta_p t_p)} \quad (8)$$

$$Y_{in1} = Y_{d1} + Y_{RLC1} = G_{in1} + jB_{in1} \quad (9)$$

$$Y_{d2} = j \frac{Y_{in1} + jY_{02} \tan(\beta_2 t_2)}{Y_{02} + jY_{in1} \tan(\beta_2 t_2)} \quad (10)$$

$$Y_{d3} = j \frac{Y_{02} + jY_p \tan(\beta_p t_p)}{Y_p + jY_{03} \tan(\beta_p t_p)} = G_{d3} + jB_{d3} \quad (11)$$

$$Y_{in} = Y_{in2} = Y_{d3} + Y_{RLC2} = G_{in} + jB_{in} \quad (12)$$

here  $Y_{RLC1}$ ,  $Y_{RLC2}$  are the admittance of the equivalent circuit of resistance film on first layer and second layer;  $Y_p$  and  $Y_{0i}$ ,  $i = 0, 1$  are the characteristic admittance of PET and PMI, respectively;  $Y_{in1}$  and  $Y_{in2}$  are the input admittance of the location ① and ②.  $B$  and  $G$  represent susceptance and conductance at the corresponding position.

The designed bi-layer absorber consists of two resistance films printed on polyethylene terephthalate (PET) with a relative dielectric constant of 3.0 and a thickness of  $t_p = 0.175$  mm and PMI foam with relative dielectric constant 1.06 and thickness  $t = 4$  mm, which shown in the Figure 2(b). The period of the unit cell is  $P = 15.2$  mm. The radius of the circular resistance film is  $R = 4.5$  mm, and the side length of the square resistance film is  $a = 14$  mm. Both the surface resistance  $R_{s1}$  and  $R_{s2}$  are equal to  $100 \Omega/\text{sq}$ . The values of the lumped elements are:  $R_1 = 144 \Omega$ ,  $L_1 = 0.1$  nH,  $C_1 = 0.219$  pF,  $R_2 = 520 \Omega$ ,  $L_2 = 6.15$  nH,  $C_2 = 0.016$  pF. The geometrical dimensions of the proposed absorber

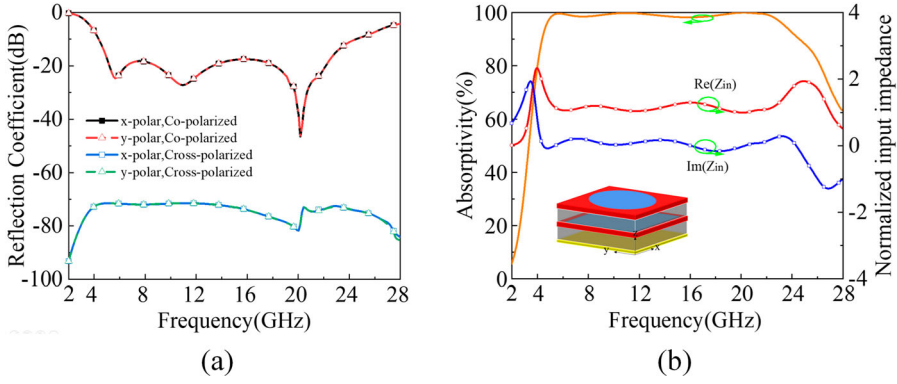


**Figure 3.** (a) co-polarization and cross-polarization of the reflection coefficient (b) Simulated absorptivity of the proposed MA and input impedance at normal incidence.

can be calculated and optimized according to the formulas in [21]. The R, C, and L are related to the structure of the resistance film and the square resistance value.

In this design, the imaginary part of the input admittance at different locations dominates the resonant frequency. As shown in Figure 2(c), the imaginary part  $B_{in1} = 0$  offers a resonant at  $f_{r1}$  and the second resonant at  $f_{r2}$  is obtained from  $B_{RLC2} = 0$ . The third resonant at  $f_{r3}$  is originated from  $B_{in} = 0$ . For the input admittance ( $B_{in} = B_{d3} + B_{RLC2}$ ),  $B_{d3} < 0$ ,  $B_{RLC2} > 0$  before the resonant frequency at  $f_{r1}$ , the first absorption resonance can be obtained at  $f_1$ ;  $B_{d3} < 0$ ,  $B_{RLC2} > 0$  before the resonant frequency at  $f_{r2}$ , the second absorption resonance can be obtained at  $f_2$ ;  $B_{d3} > 0$ ,  $B_{RLC2} > 0$  after the resonant frequency at  $f_{r2}$ , the third resonance can be obtained at  $f_3$  when  $B_{d3}$  cancels  $B_{RLC2}$ . The matching condition at resonant frequency is affected by the real part of the input admittance. Around resonant frequency  $f_2$  and  $f_3$ ,  $G_{d3}$  and  $G_{RLC2}$  play an equal role in improving the matching between the input admittance and the admittance of free space. Hence, the bi-layer absorber can offer three absorption resonance to get a wider absorption bandwidth. In Figure 2(d), the reflection curves of the designed bi-layer absorber obtained by using ECM and full-simulator have a good agreement. And it shows three resonances at  $f_1 = 5.6$  GHz,  $f_2 = 11$  GHz, and  $f_3 = 20.2$  GHz.

For the absorber, the absorption is defined as [22,23]

$$Ab = 1 - Tr - Rf = 1 - |S_{xx}^t|^2 - |S_{xy}^t|^2 - |S_{xx}^r|^2 - |S_{xy}^r|^2 \quad (13)$$

where Ab, Tr, and Rf represent absorptivity, transmission coefficient, and reflection coefficient, respectively. And the xx and xy denote co-polarization and cross-polarization. The transmission coefficient is equal to zero due to the presence of a metal plate at the bottom. Both co-polarization and cross-polarization of the reflection coefficient can be found in Figure 3(a).

The absorptivity of the designed MA is exhibited in Figure 3(b), which indicates that more than 98% broadband absorption response can be obtained at normal incidence from 4.9 to 22.6 GHz. In Figure 3(b), the normalized input impedance of the proposed MA is calculated for further explanation of the absorbing effect. According to the impedance theory

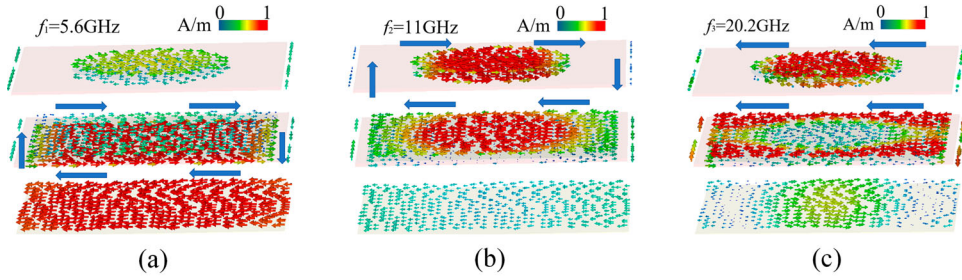


**Figure 4.** The surface current distributions of the proposed MA at (a) 5.6 GHz, (b) 11 GHz, (c) 20.2 GHz, respectively.

[14], the impedance of the absorber is calculated as

$$Z = \sqrt{\frac{(1 + S_{11})^2 - S_{21}^2}{(1 - S_{11})^2 - S_{21}^2}} \quad (14)$$

where  $S_{11}$  and  $S_{21}$  represent the reflection amplitude and the absorption amplitude, respectively. In Figure 3, the real part and imaginary part of the normalized impedance are near to one and zero in the absorption band ( $S_{11} \rightarrow 0$ ,  $S_{21} \rightarrow 0$ ), respectively, which demonstrates that the impedance of the absorber matches well with the impedance in free space.

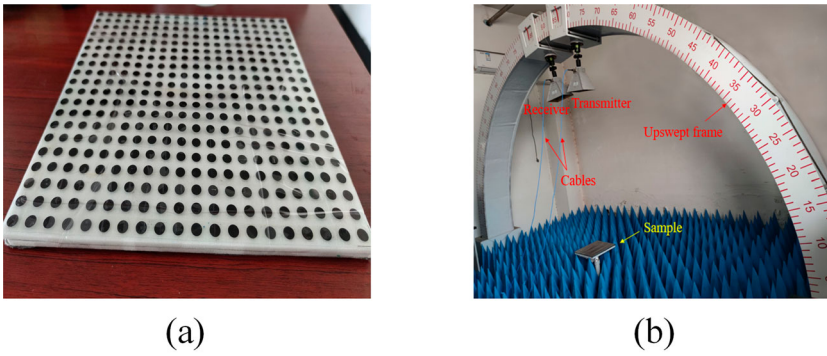
### Analysis of absorption mechanism

Figure 4 presents the surface current distribution of the designed absorber to further comprehend the absorption resonance at  $f_1 = 5.6$  GHz,  $f_2 = 11$  GHz and  $f_3 = 20.2$  GHz. The reason for the perfect absorbing effect is the coupling between the square resistance film and the metal sheet at 5.6 GHz. As shown in Figure 4(a), the directions of surface currents are reversed. Obviously, a magnetic dipole excites the magnetic resonance [18]. As shown in Figure 4(b), the perfect absorbing effect is mainly arisen from coupling the square resistance film and the round resistance film at 11.0 GHz, where a magnetic response distribution exists between layers represented by the opposite direction of surface currents. The magnetic field confinement causes Ohmic loss in the current loop to consume energy, which results in the appearance of the absorption peaks. As shown in Figure 4(c), an electric resonance exists at 20.2 GHz due to the surface current of the square resistance film and the round resistance film. Therefore, the electric resonance response is stemmed from the electric current on the square resistance film and the round resistance film layers.

### Total thickness

Under normal incidence, there is a physical minimum thickness for a nonmagnetic MA [24], calculated as:

$$d \geq \frac{\left| \int_{\lambda_{\min}}^{\lambda_{\max}} \ln |R(\lambda)| d\lambda \right|}{2\pi^2} = d_{\min} \quad (15)$$



**Figure 5.** (a) Absorber sample, (b) experimental device in a microwave chamber.

where  $R(\lambda)$  represents the reflection coefficient as a function of the wavelength  $\lambda$ . The minimum total thickness of the proposed absorber is 7.7 mm in this letter calculated by (15), and the total thickness of the proposed MA is 8.35 mm. It proves the proposed absorber closely approaches the thickness limit.

## Experimental verification and discussions

### *Insensitivity to oblique incidence*

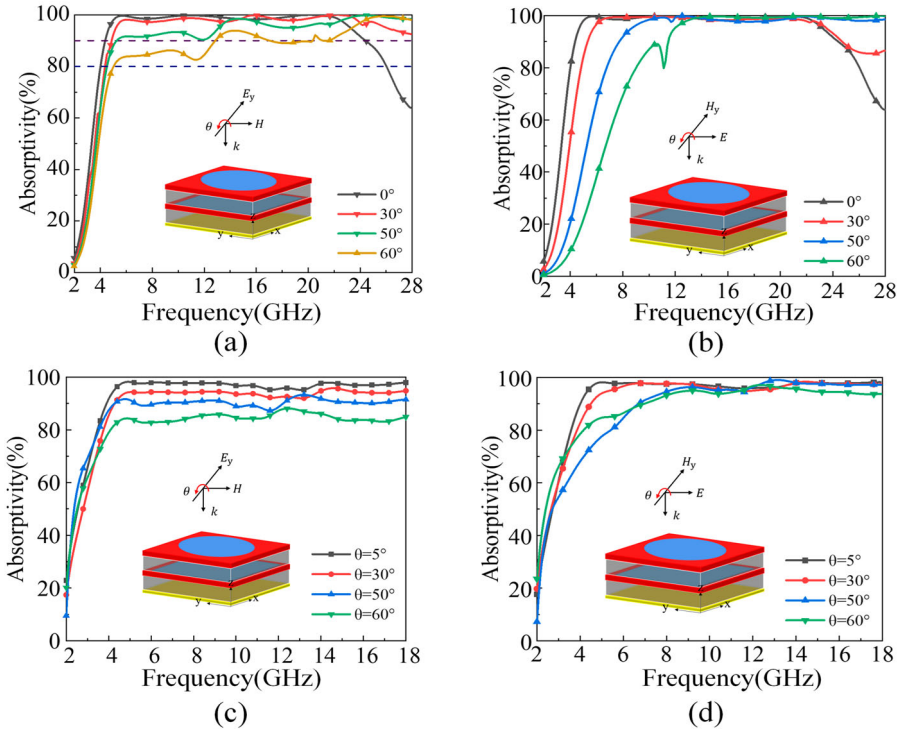
In order to demonstrate the absorptivity of the proposed MA, the entity of resistive films is fabricated on the polyethylene glycol terephthalate (PET) sheet. Different resistance values can be achieved by using inks with different conductivities. The size of the sample is  $304 \times 304$  mm including  $20 \times 20$  units, as shown in Figure 5(a). The experimental device is depicted in Figure 5(b), two broadband horn antennas are used as transmitting source and receiving source within 2–18 GHz, respectively.

Figure 6(a–d) shows the simulated and measured results with oblique incident from  $0^\circ$  to  $60^\circ$ . The absorption reaches more than 90% with bandwidth from 4.3 to 24.5 GHz (the FBW of 140.3%). Noteworthy, the absorption is greater than 98% within 4.9–22.6 GHz under normal incidence. For oblique incidence of TE and TM polarization, the absorption and working bandwidth still maintain good performance from  $0^\circ$  to  $60^\circ$ . The results exhibit polarization-insensitive absorption performance for TE and TM polarization and wide-angle stability.

### *RCS analysis*

The RCS of the same size absorber compared with PEC plate was evaluated using a full-wave simulator. Meanwhile, experimental verification is carried out. The schematic diagram of the test is shown in Figure 7(a), and the experimental setting in anechoic chamber is depicted in Figure 7(b). The transmitting antenna radiates electromagnetic wave, the receiving antenna receives electromagnetic wave, and the RCS result is calculated through algorithm of the system. Two broadband horn antennas are used as transmitting sources and receiving sources in 2–18 GHz. The RCS results of the proposed MA between simulation and measured are given in Figure 7(c). The 10-dB RCS reduction bandwidth at





**Figure 6.** Simulated absorptivity results at incident angle ( $\theta$ ) from  $0^\circ$  to  $60^\circ$  for (a) TE polarization and (b) TM polarization; Measured absorptivity results at incident angle ( $\theta$ ) from  $5^\circ$  to  $60^\circ$  for (c) TE polarization, and (d) TM polarization.  $\theta$

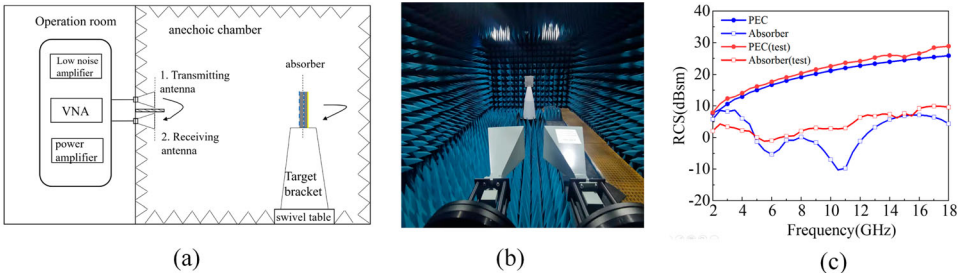


**Figure 7.** (a) RCS measure diagrammatic sketch (b) RCS measure device in a microwave chamber. (c) Simulation and measured results of monostatic RCS of the proposed absorber with frequency for TE-polarized.

normal incidence is from 4.3 to 18 GHz. The difference between the measured results and simulation ones mainly originates from measurement error.

Table 1 summarizes the absorption characteristics comparison of the proposed absorber in recent years. The designed absorber in this paper has obvious advantages from the perspective of FBW [25], thickness [26], incidence angle [27], and RCS reduction [28]. The thickness and unit size of the proposed absorber are in good level.

**Table 1.** Comparison of the metamaterial absorber with other absorber.

Ref.	Incident angle (°)	Bandwidth (GHz)/FBW (%)	Angle absorption	10 dB RCS reduction bandwidth	Thickness	Unit (mm)
[26]	0	8.2–13.4/51.1%	60° (90%)	Not reported	3 mm (0.082λ)	15.5
	30	10.5–11.7/10.8%				
[28]	0	3.75–10/91%	30° (90%)	91%	6.35 mm (0.079λ)	14
	30	6–9.34/43.5%				
[25]	0	6.95–17.4/85.8%	60° (80%)	Not reported	7.8 mm (0.18λ)	10
	60	8.1–15/59.7%				
[27]	0	3.87–14.84/117%	40° (80%)	Not reported	6.2 mm (0.19λ)	26
	40	4.25–14.84/110.9%				
This work	0	4.3–24.5/140.3%	60° (80%)	140.3%	8.35 mm (0.119λ)	15.2
	50	7.6–24.5/105%				
	60	8.8–24.5/94.3%				

## Conclusion

A MA with efficient absorption in the microwave region was designed and measured. The MA is broadband and polarization-insensitive by introducing bilayer resistance films and symmetrical structure, which absorption is greater than 98% within 4.9–22.6 GHz (the FBW is 128.7%) under normal incidence. It can maintain a good absorption performance from 0° to 60°. Besides, the absorber can reduce the monostatic RCS by more than 10 dB in the absorption bandwidth. A sample is fabricated and measured to verify absorption performance, and measurement results have good agreement with the simulation ones.

## Disclosure statement

No potential conflict of interest was reported by the author(s).

## Funding

This work was supported by National Natural Science Foundation of China [grant number 61771226].

## References

- [1] Khoshniat A, Abhari R. Metamaterial absorbers for lining system shield box and packaging: cavity analysis and equivalent material design. *IEEE Trans Electromagn Compat.* 2021 Aug;63(4):1007–1014.
- [2] Yu J, Jiang W, Gong SX. Wideband angular stable absorber based on spoof surface plasmon polariton for RCS reduction. *IEEE Antennas Wireless Propag Lett.* 2020 Jul;19(7):1058–1062.
- [3] Vafapour Z. Polarization-independent perfect optical metamaterial absorber as a glucose sensor in food industry applications. *IEEE Trans Nanobiosci.* 2019 Oct;18(4):622–627.
- [4] Wang JJ, Feng DJ, Xu ZM, et al. Time-domain digital coding active frequency selective surface absorber/reflector and its imaging characteristics. *IEEE Trans Antennas Propag.* 2021 Jun;69(6):3322–3331.
- [5] Huang H, Shen ZX. Low-RCS reflect array with phase controllable absorptive frequency-selective reflector. *IEEE Trans Antennas Propag.* 2019 Jan;67(1):190–198.
- [6] Fante RL, McCormack MT. Reflection properties of the Salisbury screen. *IEEE Trans Antennas Propag.* 1988 Oct;36(10):1443–1454.
- [7] Park MJ, Choi J, Kim SS. Wide bandwidth pyramidal absorbers of granular ferrite and carbonyl iron powders. *IEEE Trans Magnetics.* 2000 Sep;36(5):3272–3274.

- [8] Ren JY, Gong SX, Jiang W. Low-RCS monopolar patch antenna based on dual-ring metamaterial absorber. *IEEE Antennas Wireless Propag Lett.* **2018 Jan**;17(1):102–105.
- [9] Huang XJ, Liu PG, Wu Z, et al. Screen overprinted flexible radar absorber composed of planar resistor loaded metamaterials. *IEEE Antennas Wireless Propag Lett.* **2020 Aug**;19(8):1281–1285.
- [10] Shi T, Jin L, Han L, et al. Dispersion-engineered, broadband, wide-angle, polarization-independent microwave metamaterial absorber. *IEEE Trans Antennas Propag.* **2021 Jan**;69(1):229–238.
- [11] Ghosh P, Zheng C, Zhu H, et al. High-efficient photoacoustic generation with ultrathin metallic multilayer broadband absorber. *Opt Express.* **2021 Apr**;29(6):8490–8497.
- [12] Li S, Wu P, Xu H, et al. Ultra-wideband and polarization-insensitive perfect absorber using multilayer metamaterials, lumped resistors, and strong coupling effects. *Nanoscale Res Lett.* **2018 Dec**;13(386):1–13.
- [13] Sheokand H, Ghosh S, Singh G, et al. Transparent broadband metamaterial absorber based on resistive films. *J Appl Phys.* **2017 Sep**;122(10):105105.
- [14] Chen P, Kong XL, Han JF, et al. Wide-angle ultra-broadband metamaterial absorber with polarization-insensitive characteristics. *Chinese Phys Lett.* **2021 Sep**;38(2):027801.
- [15] Tirkey MM, Gupta N. Broadband polarization-insensitive inkjet-printed conformal metamaterial absorber. *IEEE Trans Electromagn Compat.* **2021 Dec**;63(6):1829–1836.
- [16] Shi T, Jin L, Han L, et al. Dispersion-engineered, broadband, wide-angle, polarization independent microwave metamaterial absorber. *IEEE Trans Antennas Propag.* **2021 Jan**;69(1):229–238.
- [17] Payne K, Xu K, Choi JH, et al. Multiphysics analysis of plasma-based tunable absorber for high-power microwave applications. *IEEE Trans Antennas Propag.* **2021 Nov**;69(11):7624–7636.
- [18] Jiang H, Yang W, Li R, et al. A conformal metamaterial-based optically transparent microwave absorber with high angular stability. *IEEE Antennas Wireless Propag Lett.* **2021 Aug**;20(8):1399–1403.
- [19] Hossain MI, Nguyen-Trong N, Sayidmarie KH, et al. Equivalent-circuit design method for wideband nonmagnetic absorbers at low microwave frequencies. *IEEE Trans Antennas Propag.* **2020 Dec**;68(12):8215–8220.
- [20] Shang Y, Shen ZX, Xiao S. On the design of single layer circuit analog absorber using double square loop array. *IEEE Trans Antennas Propag.* **2013 Dec**;61(12):6022–6029.
- [21] Hossain MI, Trong NN, Sayidmarie KH, et al. Equivalent-circuit design method for wideband nonmagnetic absorbers at low microwave frequencies. *IEEE Trans Antennas Propag.* **2020 Jan**;68(12):8215–8220.
- [22] Li SJ, Li YB, Li H, et al. A thin self-feeding janus metasurface for manipulating incident waves and emitting radiation waves simultaneously. *Annalen der Physik.* **2020 Apr**;532(5):2000020.
- [23] Li SJ, Li YB, Zhang L, et al. Programmable controls to scattering properties of a radiation array. *Laser Photonics Rev.* **2021 Jan**;15(2):2000449.
- [24] Rozanov KN. Ultimate thickness to bandwidth ratio of radar absorbers. *IEEE Trans. Antennas Propag.* **2000 Aug**;48(8):1230–1234.
- [25] Yu J, Jiang W, Gong SX. Wideband angular stable absorber based on spoof surface plasmon polariton for RCS reduction. *IEEE Trans Antennas Propag.* **2020 Jul**;19(7):1058–1062.
- [26] Nguyen TT, Lim S. Design of metamaterial absorber using eight-resistive-arm cell for simultaneous broadband and wide-incidence-angle absorption. *Sci Rep.* **2018 Apr**;8:6633.
- [27] Lim D, Lim S. Ultrawideband electromagnetic absorber using sandwiched broadband metasurfaces. *IEEE Antennas Wireless Propag Lett.* **2019 Sep**;18(9):1887–1891.
- [28] Modi AY, Balanis CA, Birtcher CR, et al. Novel design of ultrabroadband radar cross section reduction surfaces using artificial magnetic conductors. *IEEE Trans Antennas Propag.* **2017 Oct**;65(10):5406–5417.